FOURIER TRANSFORM INFRARED SPECTROSCOPY

Chapter · February 2007

DOI: 10.1007/0-387-37590-2_9

2 authors, including:

Neena Jaggi
National Institute of Technology, Kurukshetra
59 PUBLICATIONS **238** CITATIONS

SEE PROFILE

CHAPTER 9

FOURIER TRANSFORM INFRARED SPECTROSCOPY

Neena Jaggi and D.R. Vij
Kurukshetra University, Kurukshetra, India

9.1 INTRODUCTION

"Fourier spectroscopy" is a general term that describes the analysis of any varying signal into its constituent frequency components. The mathematical methods named after J.B.J. Fourier are extremely powerful in spectroscopy and have been discussed in detail [1–3]. Fourier transforms can be applied to a variety of spectroscopies including infrared spectroscopy known as *Fourier transform infrared* (FT-IR), *nuclear magnetic resonance* (NMR), and *electron spin resonance* (ESR) spectroscopy. FT-IR spectroscopy includes the absorption, reflection, emission, or photoacoustic spectrum obtained by Fourier transform of an optical interferogram. The power of the method derives from the simultaneous analysis of many frequency components in a single operation. When Fourier concepts are applied to various terms of spectroscopy, the resultant technology creates a spectrometer that gives the entire spectrum in the amount of time that a conventional spectrometer (using dispersive elements like prism and grating) would need to scan across just a single line in the spectrum. Fourier spectrometers utilizing interferometers are thus faster by a factor equal to the number of resolvable elements in the spectrum. Fourier-based methods are used over a wide spectral range [4–7]. FT spectroscopy can be employed for a long range of frequencies varying over ultraviolet, visible, near infrared, mid infrared and even far infrared regions by selecting different beam splitters and detectors for the required ranges. No other dispersive technique can be used for such a wide range of frequencies [8].

A variety of spectroscopic techniques have been used to study various samples, but FT-IR spectrometers are growing in popularity since they offer speed, accuracy and sensitivity previously impossible to achieve with wavelength dispersive spectrometers. This technique allows rapid analysis of micro-samples precise to the nanogram level in certain cases, making the

FT-IR an invaluable tool for problem solving in many studies. FT-IR spectroscopy requires some study because its principles are different from those of dispersive spectroscopy techniques and uses interferometers in the spectrometers.

In a conventional or continuous wave spectrometer, a sample is exposed to an electromagnetic radiation and usually the intensity of transmitted radiation is monitored. The energy of the incident radiation is varied over the desired range and the response is plotted as a function of frequency of the incident radiation. At certain resonant frequencies, which are characteristic of the sample, the radiation will be absorbed resulting in a series of peaks in the spectrum, which then can be used to identify the sample. In *Fourier transform spectroscopy* (FTS), instead of being subjected to varying energy of electromagnetic radiation, the sample is exposed to a single pulse of radiation consisting of frequencies in a particular range. The resulting signal contains a rapidly decaying composite of all possible frequencies. Due to resonance by the sample, resonant frequencies will be dominant in the signal; when Fourier transform on the signal is performed, the frequency response can be calculated. In this way the Fourier transform spectrometer can produce the same kind of spectrum as a conventional spectrometer, but in a much shorter time [9].

Different FT-IR spectrometers use different interferometers, such as the Michelson interferometer, lamellar grating interferometer, and Fabry-Perot interferometer. The spectrometers utilizing Fabry-Perot interferometers have low resolving power as compared to the two beam interferometers, namely the Michelson and lamellar grating interferometers. Both of the two beam interferometers have advantages and disadvantages one over the other with the basic difference being that in the Michelson interferometer division of wave amplitude takes place, whereas in the lamellar grating spectrometer division of wavefront takes place. The Michelson interferometer is often favored over the lamellar grating interferometer because of its easy construction and operation. Most of the commercially available FT-IR spectrometers use the Michelson interferometer. These have a number of advantages over the other techniques, such as high energy throughput, multiplexing, and high precision in frequency measurement. These will be discussed in detail in later sections. The principal disadvantage of FT-IR spectrometer is that from the interferometer, an interferogram is produced first rather than a spectrum, and little information is available from the interferogram without further processing. The conversion of the interferogram to a spectrum by Fourier analysis requires the use of a computer. Tremendous progress made in computer technology has allowed the method of Fourier spectroscopy to blossom. There is at present no serious technical reason that would prevent the numerical transformation of a large number of data points. Even for 10^6 sample transformations, the computation time is hardly a few seconds.

Nowadays, the main difficulty in performing Fourier spectroscopy depends upon the correct realization of the interferogram. FT-IR spectroscopy has been used as the dominant technique for measuring the infrared (IR) absorption and emission spectra of most materials [10]. The major advantage of the FT-IR technique over dispersive spectroscopy methods is that practically all compounds show characteristic absorption/emission in the IR spectral region, therefore, they can be analyzed both quantitatively and qualitatively. Although Fourier spectroscopy has been expanded in the last two decades, it still remains a new spectroscopic approach [7]. The interpretation of the effects observed in the spectrum due to features occurring in the interferogram often needs a lot of calculations in addition to Fourier transformation. The most important of these operations are apodization, phase correction, Fourier self deconvolution and curve fitting [11–15].

The far infrared region also plays an important role in the studies of low frequency molecular vibrations, derivation studies of molecular parameters via the observation of pure rotational spectra and research on molecular interactions in the solid state. The conventional IR spectrometers are not of much use for far IR region (20–400 cm^{-1}) as the sources are weak and detectors have lower sensitivity. FT-IR spectroscopy has made this energy-limited region more accessible [16, 17]. In this chapter first, the section on historical background is related to the development of Fourier transform spectroscopy. The important contributions of specific persons or groups are emphasized. In the next sections, theory, the basic integral equation used, and the various mathematical operations needed to construct the spectra from the interferogram are described. Advantages of the technique over the conventional spectrometers and some of its applications are discussed in detail in the later sections. The recent work done and the latest methodology developed are reviewed and included in the chapter.

9.2 HISTORICAL BACKGROUND

The science of Fourier transform interferometry was initiated in the late 1880s, when Albert A. Michelson invented the interferometer known as *Michelson interferometer*, on which he along with Morley, performed the well known experiment to determine the speed of light. The instrument and its uses were well received by the scientists of the day; Michelson received the Nobel Prize in Physics in 1907 for his efforts in measuring the exact speed of light and his inventions of precise scientific optical instruments [18]. As computers and electronic devices were not available back then, Michelson could not take advantage of the field of Fourier transform spectroscopy (FTS). However, using the techniques available to him, he resolved a number of doublet spectra [19]. Although Michelson knew the spectroscopic potential of his interferometer, yet the lack of sensitive detectors and nonexistence of Fourier transform algorithms were barriers for its practical application. Early

investigators faced problems in computing Fourier transforms of interferograms and were not able to invert these directly. Rather they guessed a spectrum, computed the inverse Fourier transform, and then compared it to their measured interferogram. The guessed spectrum was then modified to bring it into better agreement with the data and the process was continued until sufficient agreement was obtained [9].

Practical FTS began to come into its existence only in the late 1940s. Interferometers were used to measure light from celestial bodies and scientists produced the first Fourier transform spectrum in 1949. By this time, it was possible to calculate the necessary Fourier transforms, however, it remained a laborious and time-consuming task. At this point, besides Michelson interferometer, researchers had developed different types of interferometers, namely *lamellar grating* and *Fabry-Perot interferometers* [9]. Figure 9.1 represents a basic Michelson interferometer.

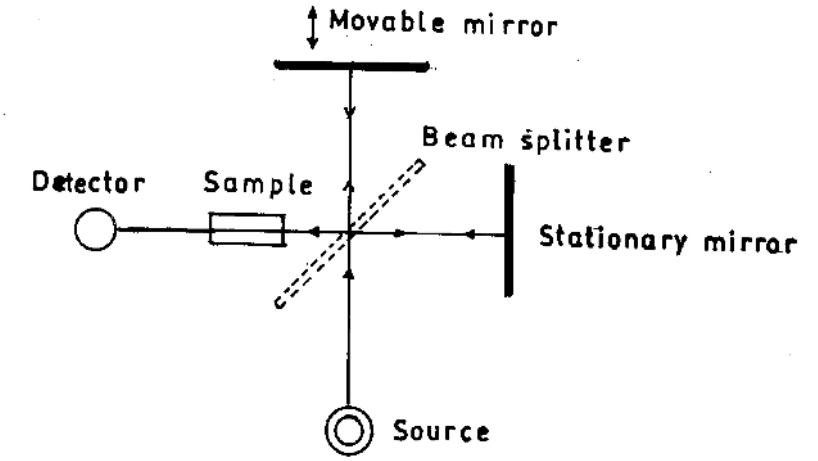

Figure 9.1 Schematic diagram of Michelson interferometer.

Lamellar grating spectrometers have much in common with the Michelson interferometer in that both are two-beam multiplex instruments of high optical throughput that produce interferograms, which are then Fourier-transformed to obtain the desired spectrum. The optical modulation device in the lamellar grating instrument is a pair of mirrors in tongue and groove arrangement as shown in Figure 9.2. When the surfaces of the two mirrors are in the same plane, they appear to be one large mirror divided into a dozen or more horizontal strips. The first mirror comprises one set of alternate strips, which are fixed, while the second mirror contains strips that are connected so they may be moved like a piston from a position forward of the fixed strips to a position behind the fixed strips [19]. In this interferometer the entire

wavefront is used, whereas the Michelson interferometer loses one half of the total flux even if the beam splitter were perfectly efficient. In the far infrared or microwave region (below 100 cm^{-1}) lamellar grating spectrometers are preferred to the Michelson interferometer because of their high efficiency.

At the onset of 1960 interest in interferometric spectroscopy was growing and that decade saw many advances in the theory of interferometric measurements and its applications to physical systems. These developments were greatly aided by the works of Cooley and Tukey [20] on the fast Fourier Transform (FFT) algorithm. This algorithm allowed Fourier transforms to be computed efficiently and easily on electronic computers available at that time. This reduced the computation time by several orders of magnitude and made the transformation from interferogram to spectrum feasible. Application of these allowed Connes and Connes [21] to record in 1966 the first near-infrared planetary spectra. Later, in 1969, they along with others [22] obtained high resolution and high quality spectra of the planets. By this time, with the advancement of computers, scientists started comparing performances of Fourier transform interferometers with grating spectrometers. Jacquinot [23] openly stated that the planetary spectra of Connes and Connes [21] if recorded by good grating spectrometers could have taken a few thousand years. This improvement in speed was possible because of minicomputers, which could carry out the fast Fourier transforms in little time. Gibbie [24] commented that computers, like photographic plates, were wonderfully sophisticated and essential spectroscopic tools, which fortunately spectroscopists did not have to invent themselves. He compared the Fourier transform spectroscopy with grating spectroscopy in this paper in a very interesting manner, and he pointed out that Fourier spectroscopy gave experimentalists a new weapon of great effectiveness.

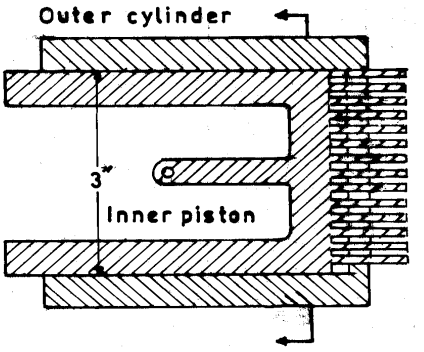

Figure 9.2 The lamellar grating modulator [19].

By 1970 commercial Fourier transform spectrometers had started to become widely accessible and the technique blossomed. However, the first FT-IR spectrometers were large and expensive and were found primarily in a few well-to-do research laboratories. Gradually, technology reduced the cost, increased the availability, and enhanced the capabilities of FT-IR spectrometers. Today Fourier transform spectrometers aided by fast computers, which perform Fourier transformation in a fraction of a second in the visible, infrared, and microwave regions, are common laboratory instruments. These are used for spectroscopic analysis in many diverse disciplines with reduced prices and increased performance.

9.3 FT–IR SPECTROSCOPY

The development and dominance of Fourier transform spectrometers over conventional spectrometers were discussed in the previous section. In the following, its basic principle, theory, and the various mathematical operations needed to generate spectrum will be discussed.

An optical system that utilizes an interferometer and a dedicated computer constitute the two basic parts of an FT-IR spectrometer. The direct acquisition of digitized infrared spectral information with the help of dedicated minicomputers has advantages. But the real advantage of an FT-IR spectrometer is obtained through the interferometer rather than the grating or prism used in the conventional spectrometers. The block diagram of an FT-IR spectrometer is represented in Figure 9.3. The three optical inputs, viz., a He-Ne laser, a white light, and the infrared source, are connected to the interferometer. All three optical signals share the same beam splitter and mirrors [25].

The computer controls optical components, collects and stores data, carries out calculations on data, and displays spectra. Because of the direct interfacing of the computer to the spectrometer, spectra can be arithmetically manipulated in an inventive way such that, for example, interfering absorbances can be eliminated by subtracting out from composite spectra the absorption bands due to interfering components [17, 26–28].

The principle of the FT-IR spectrometer is as follows: First a signal called an *interferogram* is generated by the interferometer. The interferogram obtained is a record of the signal (intensity) by the infrared detector as a function of the difference in the path for the two beams of the interferometer. The spectrum is obtained by carrying out the Fourier transform of the interferogram. In this, the intensity, which is a function of path difference x, is subjected to transformation as a whole to give the spectrum S, which depends only on frequency ν. Hence,

$$S(\nu) = \int_{-\infty}^{+\infty} I(x) e^{+i2\pi\nu x}\, dx = \mathbf{F}^{-1}[I(x)] \tag{9.1}$$

in which

$$I(x) = \int_{-\infty}^{+\infty} S(\nu) e^{-i2\pi\nu x} \, d\nu = \mathbf{F}[S(\nu)] \tag{9.2}$$

where the first integral is called the *inverse Fourier transform* and the second integral is called the *Fourier transform*. Thus, the integral given by equation (9.1) converts the interferogram $I(x)$, which is a function of path difference x to spectrum $S(\nu)$, which in turn is a function of frequency ν (from space domain to wave number domain). This calculation is carried out on a dedicated computer [29].

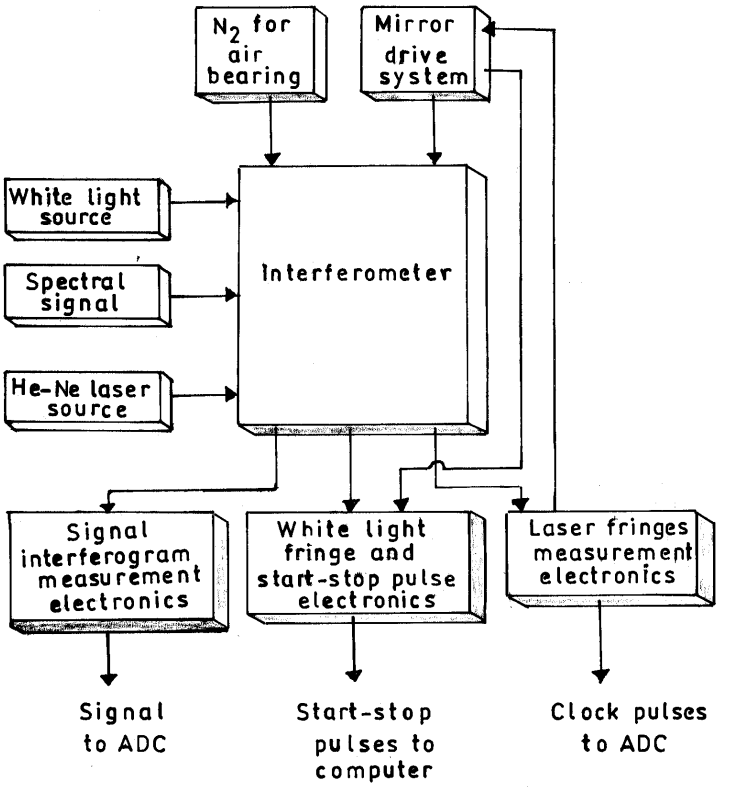

Figure 9.3 Block diagram of FT-IR spectrometer [25].

9.3.1 Basic Integral Equation

The basic integral equation used in the Fourier transform spectroscopy can be obtained from the definition of Fourier integral theorem and the principle of superposition of waves [19]. The basic equation used in the case of the Michelson interferometer can be derived mathematically as follows:

Let the amplitude of the wave (traveling in the z direction) incident on the beam splitter be given as

$$E(z,\nu)\, d\nu = E_0(\nu)\; e^{i(\omega\, t - 2\pi\nu z)}\; d\nu \tag{9.3}$$

where $E_0(\nu)$ is the maximum amplitude of the beam at $z = 0$. The amplitude of the beam is divided at the beam splitter and two beams are produced. Let z_1 and z_2 be the distances traveled by the beams when they recombine. Each beam undergoes one reflection from the beam splitter and one transmission through the beam splitter. If r and t are the reflection and transmission coefficients, respectively, of the beam splitter, then the amplitude of the recombined wave E_R is

$$E_R[z_1,\ z_2,\ \nu]\, d\nu = rt\ \ E_0\,(\nu)[\, e^{i(\omega t - 2\pi\nu z_1)} + e^{i(\omega t - 2\pi\nu z_2)}\,]d\nu \tag{9.4}$$

By definition, the intensity after recombination of the beams for the fixed spectral range $d\nu$ is given as

$$\begin{aligned} I(z_1, z_2, \nu)d\nu &= E_R(\, z_1, z_2, \nu)\; E_R{}^{*}(\, z_1, z_2\,, \nu)\; d\nu \\ &= \ 2E_0^2\left(\nu\right)\left|rt\right|^2\left[1 + \cos 2\pi\left(z_1 - z_2\right)\nu\right]d\nu \end{aligned} \tag{9.5}$$

and the total intensity at any path difference $x = (z_1 - z_2)$ for the whole spectral range is obtained by integrating equation (9.5) as

$$I_R\left(x\right) = 2|rt|^2 \int_0^\infty E_0^2(\nu)d\nu + 2|rt|^2 \int_0^\infty E_0^2(\nu)\cos(2\pi x\nu)\, d\nu\,. \tag{9.6}$$

Fourier cosine transform of equation (9.6) converts intensity into spectrum as

$$E_0^2(\nu) = \left(1/\pi\left|rt\right|^2\right)\int_0^\infty\left[I_R\,(x) - \tfrac{1}{2} I_R\,(0)\right]\cos(2\pi\nu x)dx. \tag{9.7}$$

In equation (9.7), $I_R\,(0)$ represents the flux associated with waves at zero arm displacement where the waves for all frequencies interact coherently. Thus, $I_R(0)$ is the flux associated with coherent interference and $I_R\,(x)$ is the flux associated at path difference x. $\left[I_R\,(x) - \tfrac{1}{2} I_R\,(0)\right]$ is called the *interferogram,* i.e., the oscillations of the signal about the value $\tfrac{1}{2} I_R\,(0)$. However, in various books $I_R\,\left(x\right)$ is sometimes referred to as interferogram. The spectrum $S(\nu)$, which is proportional to $E_0^2(\nu)$, can be given from equation (9.7) as

$$S(\nu) \propto E_0^2(\nu) = \text{constant} \int_0^\infty [I_R(x) - \tfrac{1}{2} I_R(0)] \cos(2\pi \nu x) dx \tag{9.8}$$

The interferogram is Fourier transformed with the help of computer to convert the space domain into the wave number domain [29]. Before discussing the steps involved to compute the spectrum from the interferogram, a brief experimental setup will be mentioned in the next section.

9.3.2 Experimental Setup

Most of the available Fourier transform spectrometers make use of Michelson interferometer, therefore, discussion will be limited to the experimental setup of the Michelson interferometer. The main differences between various FT-IR spectrometers utilizing Michelson interferometer are based on the design and the manner in which it is operated. It can be operated by scanning in a discontinuous stepwise manner (*step-scan interferometer*), a slow continuous manner with chopping of the infrared beam (slow scanning) or rapidly without chopping of the infrared beam [17]. Most of the commercially available FT-IR spectrometers make use of a rapidly scanning interferometer, which is discussed here. Figure 9.4 illustrates the schematic diagram of a rapid scanning Fourier transform spectrometer.

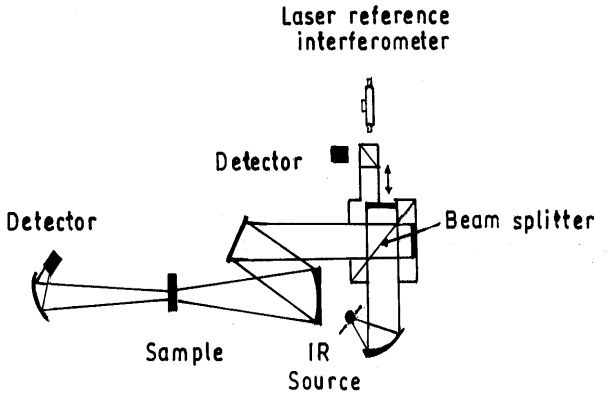

Figure 9.4 Schematic diagram of a rapid scanning Fourier transform infrared spectrometer [17].

The infrared source emits radiation of all wavelengths in the infrared region and is usually selected for desired spectral range, i.e., mercury lamps for the far infrared and glowers for the near infrared. The collimating mirror collimates the light from the infrared source. This parallel beam is then sent to the beam splitter (Fe_2O_3 in the near and far infrared regions and Ge or Si in

10,000–3000 cm^{-1}) of the Michelson interferometer. The thickness and coatings of the beam splitter must be considered carefully. The beam splitter divides the amplitude of the beam: one part of the radiation beam goes to the moving mirror and other part to the fixed mirror. The moving mirror must travel smoothly; a frictionless bearing is used with an electromagnetic drive for this purpose. The return beams from these mirrors recombine again at the beam splitter and undergo interference. The reconstructed beam is then passed through the sample (Figure 9.4) and focused on to the detector. The detector used in an FT-IR spectrometer must respond quickly because intensity changes are rapid as the moving mirror moves quickly. Pyroelectric detectors or liquid-cooled photon detectors must be used. Pyroelectric detecters have a fast response time and are used in most FT-IR spectrometers. Thermal detectors are very slow and are rarely used nowadays [30]. Pyroelectric detectors are made from a single crystalline wafer of a pyroelectric material, such as triglycerine sulphate. The heating effect of incident IR radiation causes a change in the capacitance of the material. Photoelectric detectors such as mercury-cadmium-telluride (MCT) detectors comprise a film of semiconductor material deposited on a glass surface, sealed in an evacuated envelope. Absorption of IR radiation by nonconducting valence electrons helps them to jump to a higher conducting state. This increases the conductivity of the semiconductor. These detectors have better response charactersistics than pyroelectric detectors and are used in most FT-IR instruments [31].

The motion of the mirror results in a path difference x between the two interfering beams. The path difference is twice the mirror displacement from the balanced position. The condition for maxima is $x = n\lambda$ and that for minima is $x = (n + 1/2)\lambda$, where n is the order of interference pattern, λ is the wavelength of incident radiation and ν is its frequency in cm^{-1}. Thus, each wavelength produces its own characteristic interference pattern as the mirror is displaced. For a monochromatic source there will be a cosine variation in the intensity of the combined beams at the detector. The angular frequency of the signal is $\omega = 2\pi V_m/\lambda = 2\pi V_m \nu$, where V_m is the velocity of mirror. The record of the detected signal versus optical path difference is the interferogram. Each wavelength will produce its own characteristic cosine intensity pattern of particular magnitude. Thus, for a source of many frequencies, the interferogram will be the sum of fluxes (variation of intensity) of each wavelength pattern at the detector.

To measure position and the direction of the moving mirror, the laser beam (usually an He-Ne laser) is used as shown in Figure 9.4. The laser beam undergoes the same change in the optical path as the infrared beam. Since the laser beam is monochromatic, the interferogram of the laser light will be a well-defined cosine wave. The mirror position is determined by counting the number of fringes in a highly defined laser pattern and the point of zero path length difference is obtained by finding the position of highest amplitude

intensity using the white light in place of the laser beam. For the He-Ne laser the fringe intensity will go from a maximum to a minimum with a mirror motion of λ/4 or a path difference equal to λ/2. The wavelength of the He-Ne laser is 0.6328 μm, therefore, the mirror position can be easily located to within better than λ/4 = 0.16 μm [28]. Data from the additional scans can be co-added to the data stored in the computer memory to improve the signal-to-noise ratio (*S/N*) of the interferograms because by adding a large number of scans, the noise signal present in the interferogram can be averaged out. The averaged interferogram is prepared for computation by phase correction and apodization, and then the Fourier transform is performed on the interferogram to obtain the spectrum.

The experimental method of computing a spectrum from an interferometer is as follows:

1. Measure $I_R(x)$ by recording the signal versus the interferometer arm displacement. It must be noted that $x = 2$ (arm displacement).
2. Experimentally determine the intensity of the recombined beams at zero path difference, i.e., $I_R(0)$.
3. Substitute the value of $[I_R(x) - \frac{1}{2} I_R(0)]$ in equation (9.8), and evaluate the integral for a selected value of frequency ν. The integration is performed on the computer.
4. Compute the integration of Equation (9.8) for each selected frequency ν.
5. Compute $S(\nu)$ versus ν. This gives the required spectrum.

The rapid scan FT-IR spectrometer was discussed above. In recent years, interest in step-scan FT-IR spectrometers has greatly increased [32, 33]. Many reports have appeared in the literature indicating that the technique can be a useful tool for recording the vibration spectra of a variety of time-dependent systems. The main difference in operation between step-scan and rapid-scan FT-IR spectrometers is the average velocity of the interferometer mirror, which in turn determines the effective modulation frequencies of the infrared radiation and more importantly, the modulation frequency spacing between adjacent spectral elements. In rapid-scan FT-IR spectrometers the mirror velocity lies in range 0.16–3.16 cm/s, whereas in most step-scan FT-IR spectrometers the interferometer is stepped at a rate between 1–10 fringes/sec. For more details the reader can refer to [32].

9.3.3 Advantages

There are many advantages of FT-IR spectrometers over the conventional spectrometers, but the most important advantages of FT spectrometers over earlier instruments are:

(i) higher signal-to-noise ratios for spectra recorded for the same measurement time, and
(ii) higher accuracy in frequency measurement for the spectra.

The improved signal-to-noise ratio is a consequence of both the concurrent measurement of detector signal for all the resolution elements of the spectrum known as *multiplex* or *Fellgett advantage* and of the high optical throughput of the FT-IR spectrometer known as *throughput* or *Jacquinot advantage*. The improvement in frequency accuracy of the FT-IR spectrometer is a consequence of the use of a laser, which references the measurements made by the interferometer. This is known as *laser reference* or *Connes advantage*. These advantages of FT-IR spectrometers over the dispersive spectrometers are discussed in the following sections.

9.3.3.1 Multiplex (or Fellgett) Advantage

The multiplex advantage of the FT-IR spectrometer is a consequence of the simultaneous observation of all the resolution elements $\Delta\nu$ in the desired frequency range. Fellgett [34] was the first person to transform an interferogram numerically by using the multiplex advantage, and this advantage is the well-known Fellgett advantage. In the grating or prism spectrometers, as shown in Figure 9.5, the monochromator allows only one resolution element of the spectrum to be examined at a time. Frequencies above and below this frequency band $\Delta\nu$ are masked off from the detector.

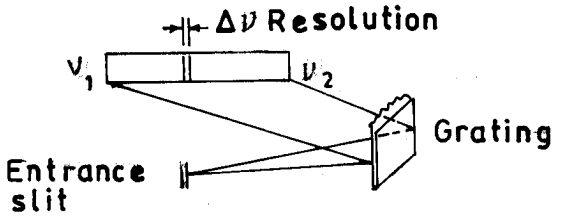

Figure 9.5 Illustration of frequency interval in a grating spectrometer [17].

The interferometer does not separate light into individual frequencies before measurement. This means each point in the interferogram contains information from each wavelength in the input signal. In other words, if 1000 data points are collected along the interferogram, each wavelength is sampled 1000 times, whereas, a dispersive spectrometer samples each wavelength only once [28]. The mathematical explanation of this is represented in the following.

Suppose one has to record a broad spectrum between the wave numbers ν_1 and ν_2 with resolution $\Delta\nu$. Let *M,* the number of spectral elements in the broad band, be represented as:

$$M = \frac{\nu_2 - \nu_1}{\Delta\nu}. \tag{9.9}$$

If grating or prism is used in the spectrometer then each small band of width $\Delta\nu$ can be observed for a time T/M, where T is the total time required for a scan from ν_1 to ν_2. Therefore, the signal received in a small band $\Delta\nu$ is proportional to T/M. If the noise is random and independent of signal level, the S/N should be proportional to $[T/M]^{1/2}$.

$$(S/N)_G \propto [T/M]^{1/2} \tag{9.10}$$

The situation for the interferometer is different because it detects in the broad band $(\nu_2 - \nu_1)$ all the small bands of resolution $\Delta\nu$ all the time. Therefore, the signal in the small band $\Delta\nu$ is proportional to T. If the noise is random and independent of the signal level, the noise is proportional to $T^{1/2}$. Thus, for the interferometer the signal-to-noise ratio is,

$$(S/N)_I \propto T^{1/2}. \tag{9.11}$$

Assuming the same proportionality constants in equations (9.10) and (9.11), the ratio of $(S/N)_I$ to $(S/N)_G$ is given as:

$$(S/N)_I/(S/N)_G = M^{1/2} \tag{9.12}$$

For a typical case $M \sim 10^4$. Thus, the signal-to-noise ratio for the interferometer is about hundred times the signal-to-noise ratio for the grating spectrometer. However, this improvement in the signal-to-noise ratio is achieved only if (i) the noise in the spectrum is only due to detector noise, and (ii) the detector noise is not proportional to the detector signal.

Studying the multiplex advantage, Voigtman and Winefordner [35] have noted that photon noise from the flux at each spectral interval contributes to the noise of each signal (or signals). Thus, a small signal may be buried in the noise from a large signal (or signals). They presented an analysis of the performance of a Fourier transform spectrometer with respect to source shot and source flicker noises. It was found that the source shot noise is uniformly distributed throughout the base whereas source flicker noise remains localized about the generating spectral region(s).

9.3.3.2 Throughput (or Jacquinot) Advantage

Like most spectroscopic techniques, the limiting aspect of infrared spectroscopy is the available energy per unit time. Infrared spectrometers should have a high energy throughput since they in particular suffer from energy-limited sources and noise-limited detectors. The increase in throughput obtainable by FT-IR spectrometers utilizing the Michelson

interferometer was first observed by Jacquinot [36] and has been universally recognized as an advantage of FT-IR spectroscopy.

Monochromators, using either gratings or prisms as dispersive elements, allow the observation of a narrow, predetermined, nearly monochromatic frequency domain. Spectra are recorded by scanning the desired frequency range at successive resolution intervals. To achieve good resolution openings of the entrance and exit slits of monochromators are made narrow, which decreases the energy entering the monochromators. This allows the detector to view only a small portion of the energy emitted by the source. Measurable signals are achieved by increasing the time of measurement per frequency interval, thereby decreasing the scanning rate. The geometric dispersion in monochromators results in throwing away most of the valuable energy [37]. On the other hand, no slit is used in the interferometer. It utilizes a collimator to focus the radiations from the source onto the sample, which means more energy gets on to the sample than is possible with dispersive spectrometers. This results in more energy passed on to the detector, increasing the signal-to-noise ratio of the spectrum recorded.

The throughput τ is defined as the product of the cross-sectional area A and solid angle Ω of the beam at any focus in the optical system. The maximum throughput of the spectrometer also determines the maximum useful $A\Omega$ of the source. For a source of given brightness, $A\Omega$ determines the total radiant power accepted by the optical system. It is, therefore, desirable to maximize the throughput and hence the energy reaching the detector so that signal-to-noise ratio is maximized [19]. One can compare the values of throughput obtainable by an interferometer and a grating spectrometer as follows:

For the Michelson interferometer, if h is the diameter of the circular infrared source and f is the focal length of the collimating mirror, the solid angle subtended by the source at the collimating mirror can be expressed as

$$\Omega_{\mathrm{M}} = \frac{\pi h^2}{4 f^2} \tag{9.13}$$

and the resolving power for the interferometer is

$$R_{\mathrm{M}} = \frac{\nu}{\Delta\nu} = \frac{8 f^2}{h^2}. \tag{9.14}$$

On substituting equation (9.14) in equation (9.13) one gets:

$$\Omega_{\mathrm{M}} = \frac{2\pi}{R_{\mathrm{M}}}. \tag{9.15}$$

If A_{M} represents the area of the collimating mirror, the throughput obtained by the Michelson interferometer is given by

$$\tau_{\mathrm{M}} = A_{\mathrm{M}}\,\Omega_{\mathrm{M}} = \frac{2\pi A_{\mathrm{M}}}{R_{\mathrm{M}}}. \tag{9.16}$$

In the case of grating spectrometers, the slit area becomes the effective source area. If A_G is the area of grating, h is the height of the slit, f is the focal length of the collimating mirror, and R_G is the resolving power of the grating then the energy throughput obtained by the grating spectrometer can be expressed as

$$\tau_G = \frac{hA_G}{fR_G}. \tag{9.17}$$

Assuming the same area and focal length for collimating mirrors used in the Michelson interferometer and grating spectrometer and the same resolving powers, the ratio of throughput for interferometer and grating spectrometers becomes

$$\frac{\tau_M}{\tau_G} \approx 2\pi\left(\frac{f}{h}\right). \tag{9.18}$$

In the best available spectrometers, (f/h) is never less than 30 (typical), therefore, $\tau_M/\tau_G \sim 190$. This means about 200 times more power can be put through the interferometer than through the best grating spectrometer. However, the theoretical value of the throughput advantage depends upon certain other factors like the detector area and efficiency of the beam splitter. Detector area must be considered because the noise level of infrared detectors increases as the square root of the detector area. Thus, a small detector area will give better signal-to-noise ratio. It is also necessary to consider the efficiency of the beam splitter. It is often expedient to use a beam splitter to obtain a spectrum in a frequency region where its efficiency is low (< 20%). Although area is unaffected by the efficiency of the beam splitter, the signal is reduced and, thus the signal-to-noise ratio at the detector will vary directly as the efficiency of the beam splitter. Increase in throughput occurs when there is a large signal at the detector. In fact, for absorption spectroscopy, which now is the dominant field of application of FT-IR, the signal in which one is interested is the one that does not make it to the detector, i.e., the absorbed light [38]. This apparently trivial statement has profound consequences, since all that we can measure is the light that is left and what we really want is the difference between it and the original light level. For higher throughput, the instrument should be designed accordingly with larger sources, beam splitter, other optical components, and the detector. While the increase in the first three only harms the performance slightly, the detector noise level increases linearly with its diameter.

Although an FT-IR spectrometer has a theoretical throughput advantage over a grating spectrometer, the numerical value of the resultant signal-to-noise improvement is dependent upon several parameters of the essential components used in the Michelson interferometer. It has been verified that photon shot noise is the ultimate limit on *S/N* measurements of optical information. It represents the ultimate limit for an ideal FT-IR spectrometer, but the performances are a good order of magnitude short of those calculated

[39]. The causes for this shortfall are not well understood. Vague suspicions about detectors, pre-amplifiers, filters, and data processing are hard to investigate.

9.3.3.3 Laser Reference (or Connes) Advantage

An FT-IR spectrometer determines frequencies by direct comparison with a visible laser output, usually a He-Ne laser. Potentially, this offers an improvement in frequency accuracy and was determined by Connes; it is also known as *Connes advantage* [21]. It has been reported that the use of a laser reference presents a foremost advantage of FT-IR spectrometers over dispersive spectrometers.

With dispersive instruments, frequency precision and accuracy depend on (i) calibration with external standards and (ii) ability of electromechanical mechanisms to uniformly move gratings and slits. By contrast, in FT-IR spectrometers the direct laser reference has the advantage that no calibration is required. Here, both the mirror movement and detector sampling are clocked by the interferometer fringes from the monochromatic light of laser. All frequencies in the output spectrum are calculated from the known frequency of the laser light. The wavenumber scale of an interferometer is derived from the He-Ne laser. The wavenumber of this laser is known very accurately and is very stable. Thus, the wavenumber calibration of interferometers is much more accurate and has much better long term stability than the calibration of dispersive instruments. One of the most important strengths of FT-IR spectroscopy lies in the ease of measuring high accuracy difference spectra. This has been feasible only because of Connes advantage, which provides accurate alignment of the spectra to be subtracted.

9.3.3.4 Some Other Advantages

Another important advantage of FT-IR spectrometers is the stray light rejection efficiency. In FT-IR spectrometers the sample is usually positioned between the interferometer and detector to take advantage of the high stray light rejection efficiency. This arrangement allows only the infrared source radiation to be modulated by the interferometer; the emission from the sample would not be modulated, therefore, would not contribute to the spectrum. Depending upon the optical design of the spectrometer, this stray light rejection advantage in not valid. Emission from hot samples can also be modulated and can produce distortions in the spectrum. Reflections from the samples also lead to distortions. These effects can be eliminated by using a half-beam blocking aperture by tilting the sample and using corner-cubed FT-IR spectrometers [40]. This can be realized in practice easily and high stray light rejection efficiency can be achieved.

Another advantage of FT-IR spectrometers is that in these, solid state electronic components are used, which are more reliable and can be easily

replaced if trouble arises. The use of a computer has the remarkable advantage of the data-handing. Computer-controlled spectral plots can be made and labeled on white paper ready for publication without the need for manual redrawing. This was not possible with dispersive spectrometers. The ability to add and subtract spectra in digital form is especially useful in eliminating interferences due to overlapping bands. This allows one to extract a maximum amount of information available in the spectrum. With the availability of increased speed and memory size of computers the use of programming in FT-IR spectrometers has also become possible.

FT-IR spectrometers are compact, simple and flexible for use in a large number of applications. The essential requirement of an FT-IR spectrometer is that the collimated beam from the source be passed through the interferometer and focused on the detector. The detector can be positioned within an experimental setup or at the end of a light pipe. To make use of the FT-IR spectrometer in various fields, some new sampling techniques such as attenuated total reflection (ATR) spectroscopy [41], photo-acoustic spectroscopy (PAS) [42], and diffused reflectance infrared fourier transform (DRIFT) spectroscopy [43] have been developed. The sample preparation is the most important feature in spectroscopic analysis. The above-referred techniques require very little sample preparation and can be used to study the samples without rigorous preparation by attaching suitable accessories with FT-IR spectrometers.

9.3.4 Other Aspects

The main objective of FT-IR spectrometers is to compute the spectrum from the interferogram. This involves a number of intermediate mathematical steps such as apodization, phase correction and Fourier self deconvolution (FSD). The excellence of the final spectrum makes these intermediate steps valuable and the use of a computer makes the operation practical. One has to devote a long time to understanding the theory of the FT-IR spectrometer, otherwise it will appear to be a black-box. Ideas about these mathematical operations are helpful for overcoming any difficulty in operating the spectrometers. A few of these are discussed here.

9.3.4.1 Apodization (or Truncation) of the Interferogram

The basic Fourier transform integral equation has infinite limits for the optical path difference (equation (9.8)), but the experimental limits are finite. The effect of this is that the truncation of interferogram occurs and is reflected in the spectrum when the interferogram is Fourier-transformed. Figure 9.6 shows the effects on spectral lineshape of various transactions of a pure sine wave.

The corrective procedure for modifying the basic Fourier transform integral is called *apodization*. In this the interferogram is usually multiplied by a function prior to Fourier transformation, which removes false sidelobes introduced into transformed spectra because of the finite limits of optical path displacement. The false sidelobes look like feet in the spectrum, so the word "apodization" is appropriate, since it means having "no feet". Codding and Horlick [11] discussed in detail the various apodization functions, which will be referred to in the further discussion. In their paper they reviewed the work done by various other researchers on apodization functions. Typical apodization functions include linear, triangular, exponential, and Gaussian truncation functions. The mathematical concept of *convolution theorem* is necessary for qualitative understanding of the truncation of the interferogram. The mathematical treatment of the convolution theorem is available in literature [1,19]. It states that the *product of the Fourier transforms of two functions is equal to the convolution of Fourier transforms of the functions and vice versa.*

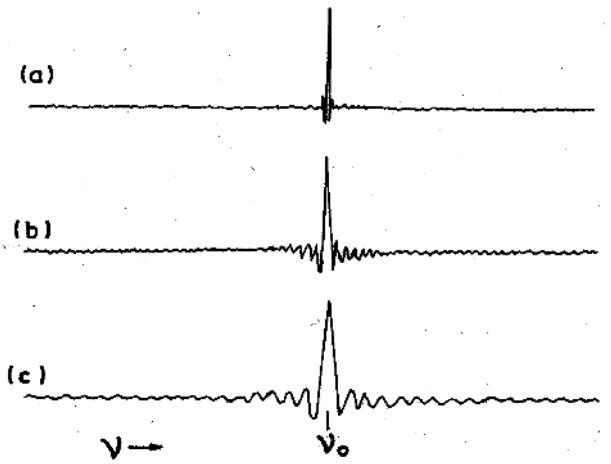

Figure 9.6 Truncated pure sine wave produced by truncating the interferogram a length equivalent to (a) 2, (b) 4, and (c) 8 cm^{-1} resolution and (a) 0.5, (b) 0.25, and (c) 0.125 cm retardation [17].

To see how apodization function is applied, first observe the effect of truncation on the spectrum of a monochromatic source. From equation (9.8) the spectrum is given by

$$S(\nu) = \int_{-\infty}^{+\infty} [I_R(x) - \tfrac{1}{2} I_R(0)] e^{-i2\pi\nu x}\, dx \tag{9.19}$$

and its Fourier transform is given by

$$\left[I_R(x) - \tfrac{1}{2} I_R(0)\right] = \int_{-\infty}^{+\infty} S(\nu) e^{+\, i2\pi\nu x}\, d\nu \qquad (9.20)$$

For the monochromatic source emitting radiation of frequency ν_1, the spectrum can be given as,

$$S(\nu_1) = \tfrac{1}{2}\left[\delta'(\nu - \nu_1) + \delta'(\nu + \nu_1)\right] \qquad (9.21)$$

where $\delta'(\nu - \nu_1)$ and $\delta'(\nu + \nu_1)$ are the Dirac delta functions. The two delta functions are used to assure that energy is conserved in going from the interferogram to the spectrum. On substituting $S(\nu)$ from equation (9.21) in equation (9.20), one gets:

$$\left[I_R(x) - \tfrac{1}{2} I_R(0)\right] = \tfrac{1}{2} \int_{-\infty}^{+\infty} \left[\delta'(\nu - \nu_1) + \delta'(\nu + \nu_1)\right] e^{+\, i2\pi\nu x}\, d\nu. \qquad (9.22)$$

Using the property of the Dirac delta function, i.e., if $f(x)$ is continuous, then $\int_{-\infty}^{+\infty} \delta'(x-a) f(x) dx = f(a)$, one gets

$$\left[I_R(x) - \tfrac{1}{2} I_R(0)\right] = 2\cos(2\pi\nu_1 x). \qquad (9.23)$$

It is clear from equation (9.23) that the interferogram of a monochromatic source is a cosine wave as shown in Figure 9.7 when the interferogram is scanned to infinity, i.e., $x = -\infty$ to $+\infty$.

The corresponding spectrum is obtained by Fourier transform of equation (9.23) as

$$S(\nu) = \int_{-\infty}^{+\infty} 2\cos(2\pi\nu_1 x) e^{-i2\pi\nu x}\, dx. \qquad (9.24)$$

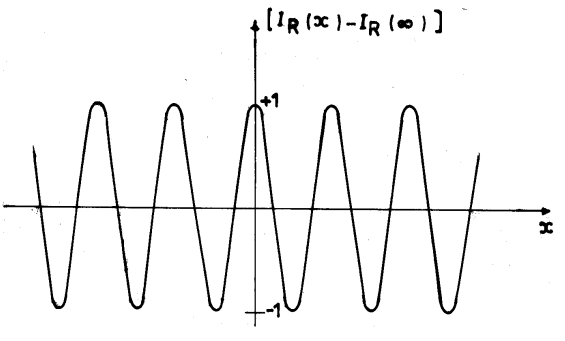

Figure 9.7 Interferogram of monochromatic source [19].

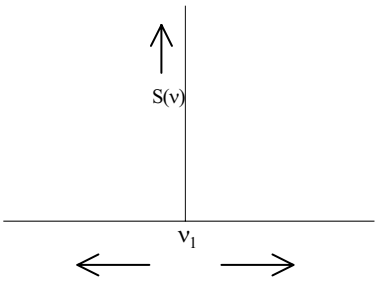

Figure 9.8 Spectrum of a monochromatic wave.

The integration of equation (9.24) results in a line spectrum at frequency ν_1 and is represented in Figure 9.8.

In actual practice, the interferogram cannot be scanned to infinity. Let the limits of x be $-L$ to $+L$. Then equation (9.24) can be written as

$$S(\nu) = \int_{-L}^{+L} 2\cos(2\pi\nu_1 x)\left[\cos 2\pi\nu x - i\sin 2\pi\nu x\right] dx$$

$$= \int_{-L}^{+L} \left(\cos 2\pi x(\nu_1 + \nu) + \cos 2\pi x(\nu_1 - \nu)\right) dx. \tag{9.25}$$

Integration of equation (9.25) gives

$$S(\nu) = 2L\left(\frac{\sin 2\pi(\nu_1 + \nu)L}{2\pi(\nu_1 + \nu)L} + \frac{\sin 2\pi(\nu_1 - \nu)L}{2\pi(\nu_1 - \nu)L}\right). \tag{9.26}$$

The first term in equation (9.26) is small, ~ 0.01 or even less, and the second term in equation (9.26) has a peak value of unity at $\nu = \nu_1$. Therefore, ignoring the first term, the spectrum of a monochromatic source produced by truncating an interferogram within a finite maximum optical path displacement L can be given as

$$S(\nu) \equiv 2L\left(\frac{\sin 2\pi(\nu_1 - \nu)L}{2\pi(\nu_1 - \nu)L}\right)$$

$$\equiv 2L(\sin z)/z \equiv 2L \operatorname{sinc} z \tag{9.27}$$

where $z \equiv 2\pi(\nu_1 - \nu)L$. $2L$ sinc z is usually known as *instrument lineshape function* (ILS). The plot of the spectrum given by equation (9.27) is represented by a solid line in Figure 9.9.

Therefore, when an interferogram is scanned to finite limits, sinc z represents the spectrum of the monochromatic beam. The sidelobes or feet appear below the baseline. The central peak has a finite width as well. The feet appear as false sources of energy at nearby wavelengths. The process of apodization reduces the size of these feet. This can be carried out using different functions. Let the interferogram be corrected first by multiplying it with a triangular function $\Lambda = 1 - |x|/L$, then the spectrum will be given by

$$
\begin{aligned}
S(\nu) &= 2\int_{-L}^{+L}\left(1-\frac{|x|}{L}\right)\cos(2\pi\nu_1 x)e^{-i2\pi\nu x}\,dx \\
&= 2\int_{-L}^{+L}\left[\left(1-\frac{|x|}{L}\right)\cos\left[2\pi(\nu_1-\nu)x\right]\right]dx \\
&= 2\left\{\frac{1-\cos[2\pi(\nu_1-\nu)L]}{[2\pi(\nu_1-\nu)]^2 L}\right\} \\
&= 2\cdot\frac{2}{4}\frac{\sin^2\pi(\nu_1-\nu)L}{\left(\pi(\nu_1-\nu)L\right)^2}L \\
&= L\frac{\sin^2\pi(\nu_1-\nu)L}{\left(\pi(\nu_1-\nu)L\right)^2} \qquad (9.28)
\end{aligned}
$$

Let $\pi(\nu_1-\nu)L = z/2$, then

$$S(\nu) = L\,\mathrm{sinc}^2(z/2). \qquad (9.29)$$

This function is plotted in Figure 9.9 by the dotted curve. It clearly indicates that the triangular apodization function on the interferogram reduces the feet or sidelobes. There is an increase in the width of the central peak but to a small extent. Here only the triangular apodization has been considered. Some other functions such as cosine, trapezoidal, Gaussian, etc., can also be used for apodization. From equations (9.27) and (9.29) it is clear that L appears in the spectrum, so one must take the same L for recording the background as well as the sample spectrum.

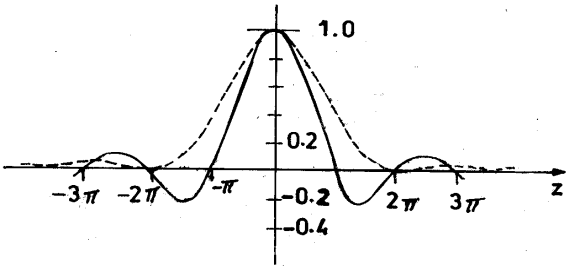

Figure 9.9 Plots of (1) sinc z = (sin z)/z versus z and (2) $\mathrm{sinc}^2\, z/2$ versus z [17].

Now, with the help of a boxcar function it will be shown that the spectrum computed for a finite optical path difference is the convolution of the idealized spectrum produced by infinite optical path differences with the

instrument lineshape function. Let $I_R(\infty)$ be the flux associated for infinite arm displacement, which corresponds to the incoherent interference. For the Michelson interferometer (the two-beam interferometer), the ratio of fluxes of incoherent interference and coherent interference is ½, i.e.,

$$\frac{I_R(\infty)}{I_R(0)} = \frac{1}{2}$$

or ½ $I_R(0) = I_R(\infty)$. Using this in equation (9.19), the idealized spectrum for infinite optical path difference and the instrumental spectrum for the finite optical path difference can be represented by equations (9.30) and (9.31), respectively:

$$S(\nu) = \int_{-\infty}^{+\infty} \left[I_R(x) - I_R(\infty) \right] e^{-i2\pi\nu x} dx \tag{9.30}$$

$$S_I(\nu) = \int_{-L}^{+L} \left[I_R(x) - I_R(\infty) \right] e^{-i2\pi\nu x} dx. \tag{9.31}$$

Let the rectangular function, or so-called boxcar function [44], be defined as

$$rect(x) = \begin{pmatrix} 1, & |x| \le L \\ 0 & |x| > L \end{pmatrix}. \tag{9.32}$$

Applying this boxcar function, the instrumental spectrum from equation (9.31) becomes

$$S_I(\nu) = \int_{-\infty}^{+\infty} \left[I_R(x) - I_R(\infty) \right] \text{rect}(x) e^{-i2\pi\nu x} dx. \tag{9.33}$$

Taking the Fourier transforms of $S_I(\nu)$ and $S(\nu)$ given by equations (9.33) and (9.30), respectively:

$$\mathbf{F}[S_I(\nu)] = [I_R(x) - I_R(\infty)] \text{ rect } (x) \tag{9.34}$$

$$\mathbf{F}[S(\nu)] = [I_R(x) - I_R(\infty)] \tag{9.35}$$

Let function $G(\nu)$ be another function defined such that its Fourier transform is the rectangular function, i.e.,

$$\mathbf{F}[G(\nu)] \equiv \text{rect } (x) \tag{9.36}$$

Using equation (9.36) in equation (9.34) one gets

$$\mathbf{F}[S_I(\nu)] = \mathbf{F}[S(\nu)]\, \mathbf{F}[G(\nu)] \tag{9.37}$$

Applying the convolution theorem here, which states that product of the Fourier transforms of two functions is equal to the Fourier transform of the convolution of two functions, then equation (9.37) can be written as:

$$\mathbf{F}\,[S_I\,(\nu)] = \mathbf{F}\,[S\,(\nu) * G\,(\nu)] \text{ or } S_I(\nu) = S(\nu) * G(\nu) \tag{9.38}$$

Using equations (9.32) and (9.36), the Fourier transform $G(\nu)$ of the rectangular function is given by:

$$\begin{aligned} G(\nu) &= \int_{-L}^{+L} e^{-i2\pi\nu x}\, dx = 2L\,\sin(2\pi\nu L)/(2\pi\nu L) \\ &= 2L\,\mathrm{sinc}(2\pi\nu L) \end{aligned} \tag{9.39}$$

which is the instrument lineshape function (ILS).
Therefore, $S_I(\nu) = S(\nu) * (\mathrm{ILS})$.

Thus the instrumental spectrum is given by the convolution of the ideal spectrum with the instrumental lineshape function. This can be applied to find the Fourier transform of the truncated sine wave, which is the product of the sine wave of infinite extent and a box function of width $2x_{max}$ and is represented in Figure 9.10.

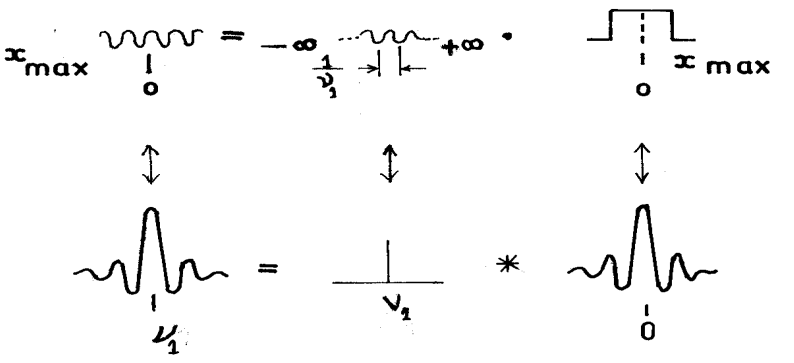

Figure 9.10 Illustration of the convolution theorem to show the effect of truncating an interferogram [17].

The Fourier transform of the infinite sine wave in distance space is just a delta function in frequency space at the value of the sine wave frequency. The Fourier transform of a boxcar function of width x_{max} is a function $\sin(2\pi x_{max}\nu)/(2\pi x_{max}\nu)$. This is by definition just $\mathrm{sinc}\,(2\pi x_{max}\nu)$. The convolution of $\mathrm{sinc}(2\pi x_{max}\nu)$ with the delta function is the mathematical equivalent of allowing the sinc function, to sweep over the line to generate a new function. This gives another sinc function, which is the Fourier transform of the truncated sine wave (Figure 9.10).

Figure 9.11 shows the instrument line function resulting from a triangular apodizing function using the convolution theorem.

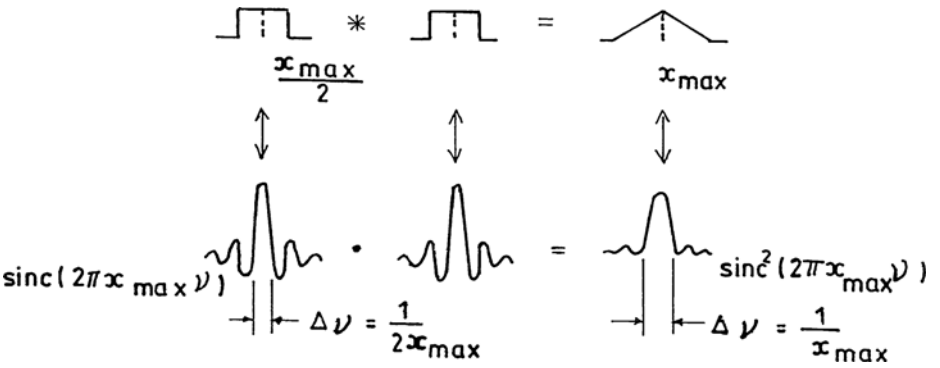

Figure 9.11 Instrumental line function resulting from a triangular apodization function using the convolution theorem [17].

9.3.4.2 Phase Information and Phase Correction

The phase information of interferograms is another important aspect of the conversion of interferograms to spectra [11]. The term "phase" refers to the phase of the individual frequencies that make up the interferogram. The phase of the frequencies may be calculated at any point on the interferogram, whereas the phase information is most easily interpreted if it is calculated at the point on the interferogram where the central maximum occurs. When calculated in this manner, the phase is said to be referenced to the central maximum. At this point the phase is stationary, i.e., all the frequency components of the interferogram have approximately the same phase and generate the central fringe maximum. The phase components of the Fourier transforms of the interferogram give information about the sample. Kawata et al. [13] developed a new idea of spectral library-searching in which only the phase components of Fourier transforms of both the sample and the reference spectra are used for spectral identification. This method has a high discrimination ability for distinguishing between similar spectra, and is very resistant to peak height variation and peak position shift due to experimental conditions. Figure 9.12 shows the spectra of toluene and benzene reconstructed from phase-only Fourier representation.

An ideal interferogram should be symmetric about the point of zero path length difference and on digitization should contain a data point at the peak of the interferogram. However, in general the interferogram is not symmetric around the strong peak at zero path difference because all the frequency components of the wave do not reach their maxima at exactly the same time. This may be due to improper construction of the beam splitter, which causes short wavelengths to be advanced or retarded with respect to long wavelengths and frequency-dependent delay in phase introduced by the detector. A correction for this asymmetry is obtained by a linear function that gives the relationship between the phase shift and the frequency [17].

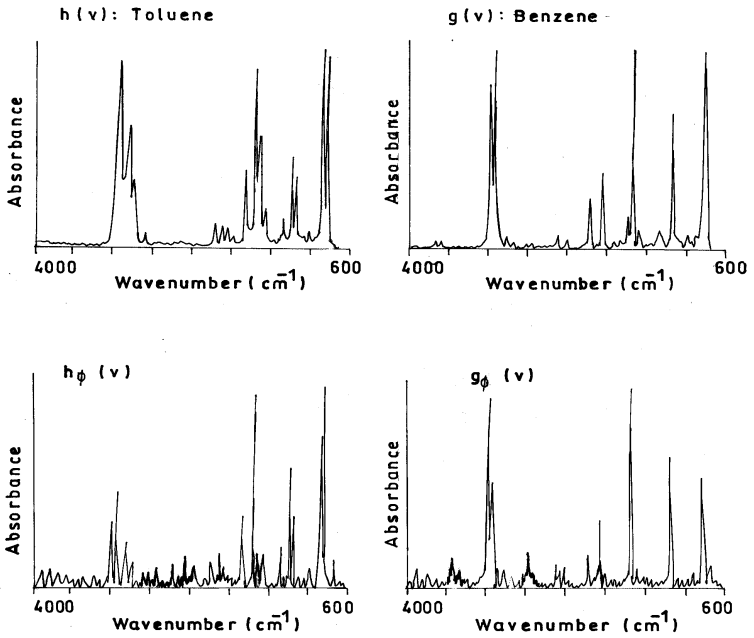

Figure 9.12 Spectra of toluene and benzene reconstructed from the phase-only Fourier representation [13].

9.3.4.3 Fourier Self-Deconvolution

The interpretation of spectral data is often impeded by the effect of overlapping bands. Earlier the mathematical technique known as *curve-fitting* was used for separation of overlapping bands. The scope and limitations of this technique were discussed in detail by Maddams [45]. Nowadays, *Fourier self-deconvolution* (FSD) is coming into increasing use as a method for band sharpening and a means for peak-finding in systems of overlapping infrared bands whose widths are significantly greater than the instrumental resolutions. This is the predominant case in a solution phase spectra, where bands are broadened because of intermolecular interactions and exhibit Lorentzian contours [46]. The method was put on a sound basis by Kauppinen and coworkers [15].

Application of FSD involves measurement of a spectrum followed by Fourier transformation of the region of interest back to the interferogram stage. If the original spectrum had bands of Lorentzian contour, the corresponding interferogram would be a sum of exponentially decaying cosine waves. The exponential decay is removed by multiplying the sum with an increasing exponential function, thus producing an interferogram of more cosinusoidal components. Fourier transform at this point is performed again, which regenerates the original spectrum but with significantly narrow

bandwidths. This effectively resolves some overlapping features, although the signal-to-noise ratio is degraded by this process [44]. FSD offers some important advantages over other resolution enhancement techniques. The derivative technique, although effective, produces artifacts of opposite sign relative to the true features. The curve-fitting technique requires extensive user input and can produce highly subjective results. FSD, on the other hand, requires minimal user input. The two parameters that must be input, are bandwidth (full width at half maximum) and a parameter related to the factor by which bandwidths are to be narrowed. The optimal values for these parameters has to be determined since a bandwidth set too large will produce negative features, while a value of the factor by which bandwidths are to be reduced, if set too large, will produce excessive noise. Figure 9.13 shows the application of the technique to resolve the two overlapping bands.

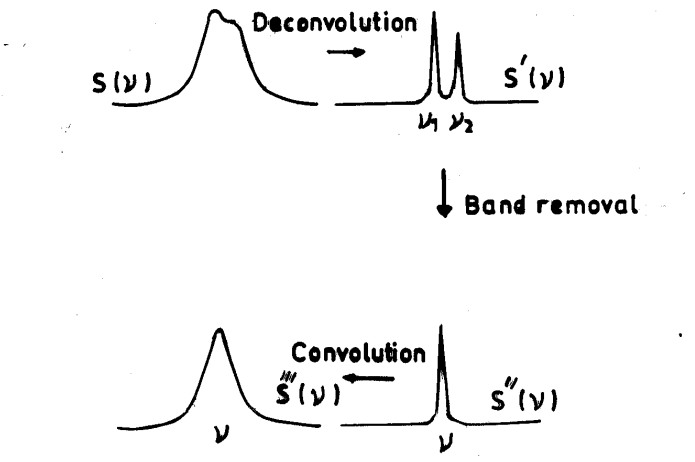

Figure 9.13 Illustration of band separation by deconvolution [15].

9.4 APPLICATIONS

Applications of FT-IR spectrometers are tremendous in almost every field, such as industry [47–51], research [52–55], and medical science [56–58]. Breakthroughs in analytical spectroscopic instrumentation in the last few decades have dramatically boosted its qualitative and quantitative analytical potential. The joint use of the FT-IR spectroscopic technique and suitable software for calculations allows one to fully exploit the vast amount of information contained in the IR spectra for organic substances with a view to

the simultaneous resolution of complex mixtures. The widest use of FT-IR spectrometers is mainly in industry because here they are able to provide useful information in both time and frequency domains. Therefore, large amounts of data can be analyzed with high precision in a very small time. Nowadays microbeam FT-IR spectrometers allow spectra from a very small sample (a few nanograms) of material to be obtained quickly with little sample preparation. For many companies this is important economically since it results in more data at a lower cost for some materials; thin films of residue are identified with sensitivity that is highly competitive with electron- or ion-based surface analysis techniques. This is mainly achieved by measuring the attenuated total reflection from the material's surface. Areas as small as 10–15 microns can be analyzed. The technique has also been used to measure surface temperature, which is independent of material emissivity, surrounding radiation sources, and instrument calibration, as shown by Markhan et al. [49]. This use has applications in power generation, metal processing, chemical production, and many other areas. Many companies use FT-IR as an aid in the precise determination of the chemical identity of organic contamination in the disk drive, and also in biomedical and semiconductor industries. FT-IR spectroscopy can be used as a rapid and nondestructive technique for determination of constituents in many samples. The technique is a fast and cost effective tool for routine monitoring of multiple constituents such as sucrose, glucose, fructose, citric acid, etc. in the production of common juices, for example [59, 60]. Very recently, Van de Voort et al. [61] developed a practical FT-IR method to determine the moisture contents in lubricants, which has advantages in terms of sample size, speed, and the variety of oil types that can be handled. This technique has also been employed by Stewart [62] to study plant tissues. This allows the study of localized changes in cell wall composition and structure of individual cells and comparison of those with different and distant tissues. This was not possible with other spectroscopic techniques. Though there is a long list of areas where FT-IR spectrometers can be used (in identification of polymers, to confirm composition of raw materials, to verify compound composition, in surface analysis, in micro-contamination identification, in forensic departments, for quality control screening, in biomedical science, in semiconductor industry, etc.), yet the limiting applications of FT-IR spectrometers will be discussed which are of current interest. These will include studies made on atmospheric pollution, planetary atmospheres, optical fibers, as well as surface studies, and the study of polymers and bio-molecules.

9.4.1 Atmospheric Pollution

Atmospheric pollution is one of the greatest problems worldwide due to increase in the number of industries, oil refineries, vehicles, and so on. Atmospheric pollutants are very destructive. These damage crops and buildings and cause serious health problems to inhabitants. Therefore, it is essential to monitor these precisely. As the concentration of the air pollutants is very small—of ~ ppm (parts per million) level or even less such as of ~ ppb (parts per billion)—so a very sensitive method is required to record their presence in air. The advantages of FT-IR spectroscopy can be utilized to take the spectrum of polluted air (near factories or ponds, etc.), which can show the presence of pollutants even if their concentration is of the order of ppm or less. The fast and the intensive development of FT-IR spectroscopic technique has propelled the progress of trace gas analysis of the atmosphere. Basick et al. [10] reviewed the results of the most significant contributions in this field by FT-IR spectroscopy. The techniques reviewed include *in situ* IR absorption measurements over open paths in the field, such as remote sensing using the sun, the sky or natural hot objects as IR source of radiation and also IR emission measurements of hot trace gas sources, e.g., stack emissions, exhaust gases of combustion sources, and other industrial effluents.

The measurements of gaseous air pollutants by infrared absorption has been possible only through the use of multiple reflection long path cells or by some remote sensing instruments. The detectors used should be highly sensitive and nitrogen-cooled. The fundamental problem in investigating gaseous atmospheric pollutants is the detection of small concentrations at partial pressures as low as 10^{-8} atm (or lower). Therefore, it is necessary that these have strong infrared bands that do not overlap with water or CO_2 absorption bands. It becomes essential to concentrate the pollutant first by a separation technique that separates it from nitrogen, oxygen, water vapor, and CO_2. Hanst and coworkers [63] developed a separation technique operating on the principle of vapor pressure differences. At low temperatures, the vapor pressure of pollutants are lower than the vapor pressure of nitrogen and oxygen. Cryogenic condensations followed by distillation can be used for concentrating the pollutant molecules. CO_2 can be absorbed chemically. Trace gases in the atmosphere have been measured at 10^{-11} atm using this concentration technique along with long-path infrared spectroscopy. The cell used by Hanst and coworkers and the spectrum of the polluted air [64] are shown in Figures 9.14 and 9.15 respectively.

The spectrum between 700–1200 cm^{-1} shows identifiable bands of eleven species of pollutants in addition to the naturally occurring nitrous oxide. Here the spectrum subtraction routines are applied to obtain the presence of weaker bands, which is a characteristic of Fourier transform spectrometers. In the upper spectrum, the dominant bands of acetylene, trichlorofluoromethane, dichlorodifluoromethane, ethylene, and nitrous oxide have been subtracted so

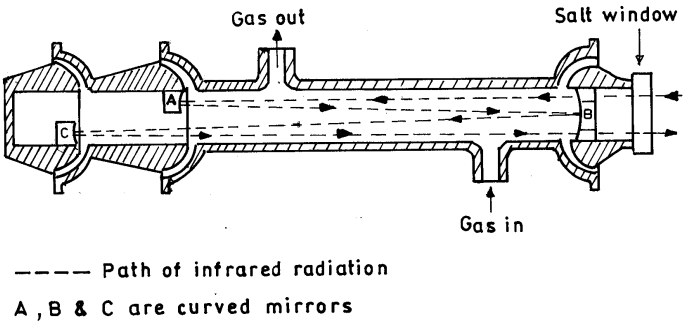

Figure 9.14 Multiple-pass cell with ball joint mounting of mirrors [64].

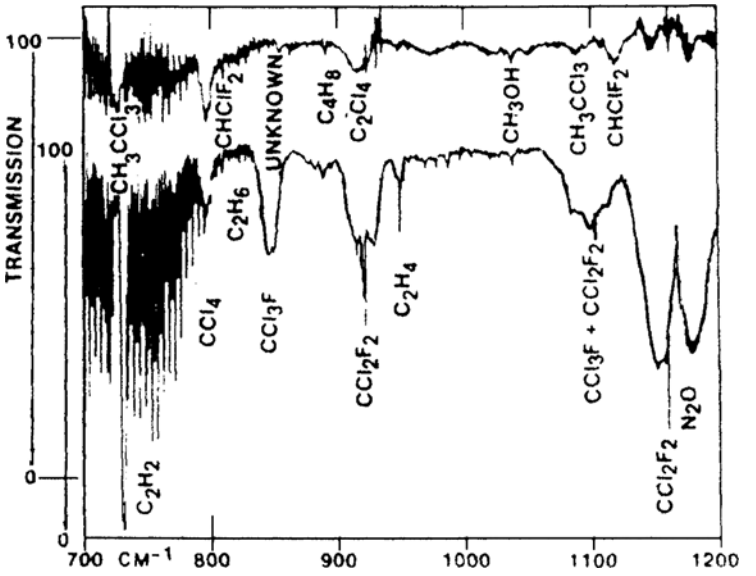

Figure 9.15 Spectra of pollutants recorded utilizing the cryogenic concentration technique [64].

that weaker bands of other pollutants could be measured which otherwise were hidden in the strong bands of other pollutants.

Nowadays, with the advancement in instrumentation, the scenario is quite different. Hong and Cho [65] used *open-path FT-IR* (OP-FT-IR) spectrometry, which improves the temporal and spatial resolution in air pollutant measurement over the conventional methods. However, a successful OP-FT-IR operation requires an experienced analyst to resolve chemical interference as well as derive a suitable background spectrum. Recently Kraft et al. [66] developed an FT-IR sensor system for the continuous determination of a range of environmentally relevant volatile organic compounds in sea water. They developed a prototype of a robust, miniaturized FT-IR spectrometer for

in situ underwater pollution monitoring. The assembled instrument is enclosed in a sealed pressure vessel and capable of operation in an oceanic environment down to depths of at least 300 m. They detected a range of chlorinated hydrocarbons and monocyclic aromatic hydrocarbons in sea water down to a concentration level of ppb.

9.4.2 Study of Planetary Atmosphere

Planetary atmospheres consist of chemical systems that can be observed remotely or directly sampled with entry probes. Earlier it was possible only to study the atmosphere of our planet earth with the spectroscopic techniques. With the advent of FT-IR spectroscopy, it is possible to explore the atmosphere of every planet, satellite, or asteroid. FT-IR spectrometers have been shown to offer significant improvements over classical dispersive methods in the study of infrared spectral features in astronomical measurements [67]. These improvements result from the three well known advantages of the technique, i.e., spectral multiplexing, high throughput, and significantly improved wavenumber scale.

Fourier transform infrared spectrometers used for astronomical observations differ in some important ways from their laboratory counterparts. The most evident difference is seen in the need to interface the spectrometer to the telescope optics and to minimize its response to the thermal radiation background and to the fluctuations in atmospheric transmission. The spectroscopist in the laboratory can change the brightness of the source or repeat the experiment a number of times. But an astronomer has to complete the experiment in limited time and there is no opportunity to repeat the experiment. Thus the astronomical Fourier spectroscopist pays stress on high optical efficiency, optimal conversion of observing time into integration time, and high levels of stability and reliability of all components of the spectrometer. Although the spectra of Venus were recorded by Connes [21] in 1966 and still earlier in 1962 by grating spectrometers, the real analysis could only be made in 1965 with the advancement of the technique and availability of computers [68]. A section of spectra of Venus observed with various instruments by different scientists is shown for comparison (Figure 9.16).

It is clear from Figure 9.16 that many weak lines between the major CO_2 lines are also visible. A comparison of Figure 9.16a with Figure 9.16d shows the advantages (multiplex) of FT-IR spectrometers as both spectra had been recorded using the PbS detector with approximately the same detector sensitivity. Further studies of FT-IR spectra of Venus showed the presence of water. Figure 9.17 shows a section of the Venus spectra obtained by an improved interferometer having resolution 8 cm^{-1}, carried by flights of CV999 by National Aeronautics and Space Administration (NASA). These spectra were analyzed using the technique of curve-fitting [68]. The spectrum

shows several CO_2 bands marked on the Figure 9.17 and the 1.9-μm water vapor band in Venus's atmosphere.

The atmospheric spectra of all the planets have been recorded. The studies can be broadly divided into two categories, viz., that of terrestrial planets which comprise of Mercury, Venus, Mars, and the moon (which defines earth's atmosphere) and major planets, which include Jupiter, Saturn, Uranus, and Neptune. The difference between the terrestrial planets and the major planets is that of densities of the materials present on the two groups of planets. The density of the terrestrial planets is due to a mixture of rocky materials (silicates) and the density of the major planets is due to the presence of light elements like hydrogen and helium. Comparative spectra of the four terrestrial planets and the major planets are shown in Figures 9.18 and 9.19, respectively. Strong methane absorptions are observed in the spectrum of the major planets. A laboratory spectrum of CH_4 is also shown in Figure 9.19e. The spectrum of Jupiter has additional absorptions due to presence of NH_3 gas at 1.5 μm.

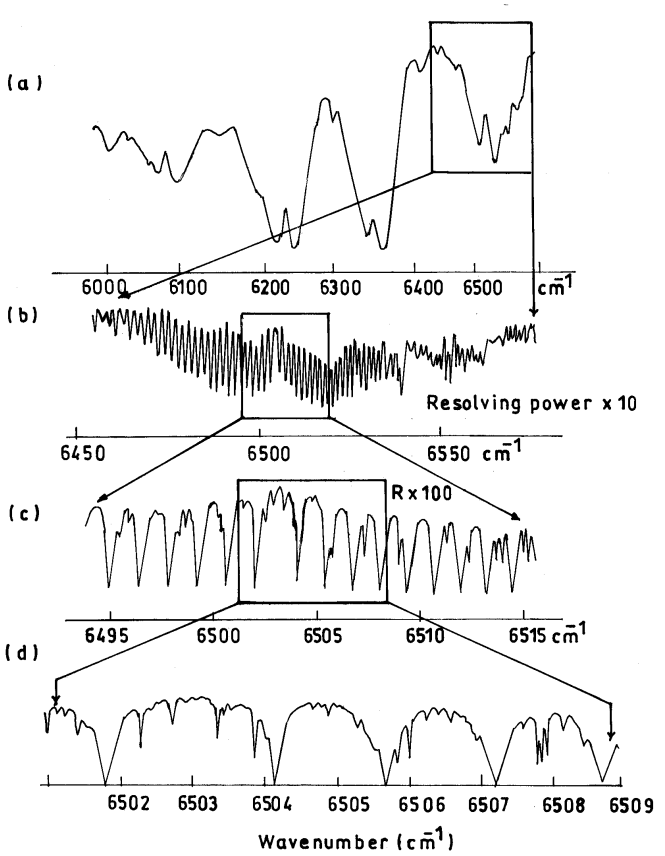

Figure 9.16 Sections of Venus spectra (a) by grating, (b) the first FT-IR spectra by Connes and Connes (1966), (c) an excerpt of the Connes et al. (1969) and (d) spectra recorded by Connes and Michal (1975) [68].

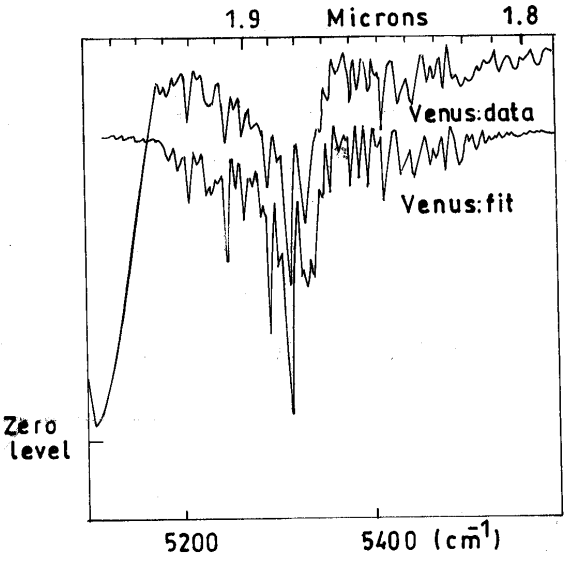

Figure 9.17 A section of the Venus spectra at resolution 8 cm^{-1} [68].

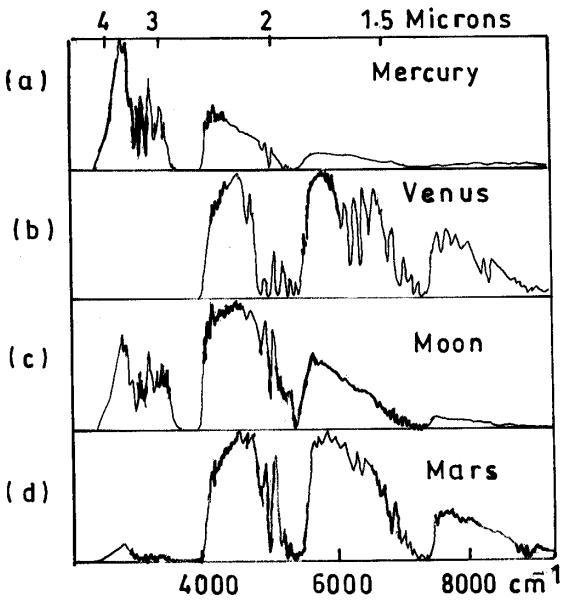

Figure 9.18 Comparative spectra of the terrestrial planets [68].

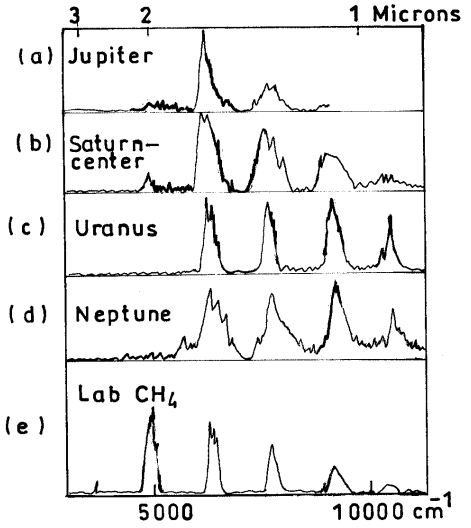

Figure 9.19 Comparative spectra of the major planets and CH_4 [68].

Recently, the planetary Fourier spectrometer on the European Space Agency's Mars express spacecraft was used to investigate the chemical composition of the Martian atmosphere. It is capable of measuring the distribution of the major gaseous components of the atmosphere, the vertical distribution of temperature, and the pressure and determining their variation and global circulation during the different Martian seasons.

9.4.3 Surface Studies

These days, much attention has been paid to studies of thin films deposited on solid substrates for microelectronics applications [69]. This interest largely lies in the potential applications of ordered nanostructures in a number of fields such as molecular electronics, nonlinear optics, and sensors. The FT-IR spectrometer allows us to handle data in a variety of ways. The study of thin films becomes more reliable and efficient by FT-IR spectrometers than by any other technique. Vibrational spectroscopy by FT-IR instruments in particular has been applied successfully to such films deposited on a flat metal substrate using reflection-absorption spectroscopy (RAS) and attenuated total reflectance (ATR). Sometimes, a transmission spectrum is needed if detailed information about a molecular spectrum is required [70]. ATR and RAS give a quasi-absorption spectrum which is not identical but is similar to a transmission spectrum, the interpretation of results may be much easier than in the case for other reflection techniques, which give dispersive spectra [69]. In addition, these techniques facilitate sample preparation and an

enhancement is often observed with respect to transmission under proper conditions.

As the quality of spectra has improved with the progress of instrumentation, it has become possible for one to observe the reflection spectra for even a single monolayer on dielectric materials; however, interpretation of the spectra becomes difficult due to optical effect. It has been shown that it is possible to determine the thickness of the thin surface layers by FT-IR/ATR spectroscopy. A method was proposed by Ohta and Iwamoto [71] to give the relation between thickness of the probed surface layer and absorbance in FT-IR/ATR spectroscopy.

9.4.4 Characterization of Optical Fibers

Optical fibers are becoming increasingly important in the areas of data communication and sensing as advantage is taken of their low attenuations, which result in little signal loss over long distances of fibers. However, the fiber attenuations are wavelength-dependent and there are spectral regions where the fibers have lower attenuations as well as areas where the light losses are very severe. In order for one to select the best regions for transmission, the fiber must be well characterized spectroscopically [72]. The FT-IR spectrometer offers considerable attraction as an instrument for the characterization of optical fibers.

Lowry et al. [73] have developed an accessory for FT-IR spectroscopy to measure the spectral response from various types of optical fiber cables. The study has proved to be important for use in fiber-optic sensor-based applications. This work has made extensive use of the flexibility of the FT-IR spectrometer, and easily changed optical components to allow for rapid measurements without changing the position of the optical fiber under investigation.

In recent years optical fiber-based biosensors have been developed and are used in biomedicine and biotechnology [74]. The measurement of amounts of biomolecules such as proteins in solutions is one of the numerous applications of these biosensors. Most recently Kraft et al. [66] and Steiner et al. [75] used fiber-optic cables to develop a fiber-optic sensor system, which can be used to measure sea water pollution with concentration of the order of ppb by FT-IR spectrometers. Sol-gel coated fiber-optic sensors have also been developed and the spectroscopic properties of this important class of fibers have been monitored by FT-IR technology [76].

9.4.5 Vibrational Analysis of Molecules

The absorption of IR radiation is associated with the vibration of chemical bonds, therefore, the absorption spectrum contains a wealth of information about the vibrational levels of the molecule. Infrared spectra of n-alkanes and branched alkanes have interested a number of workers during the last few

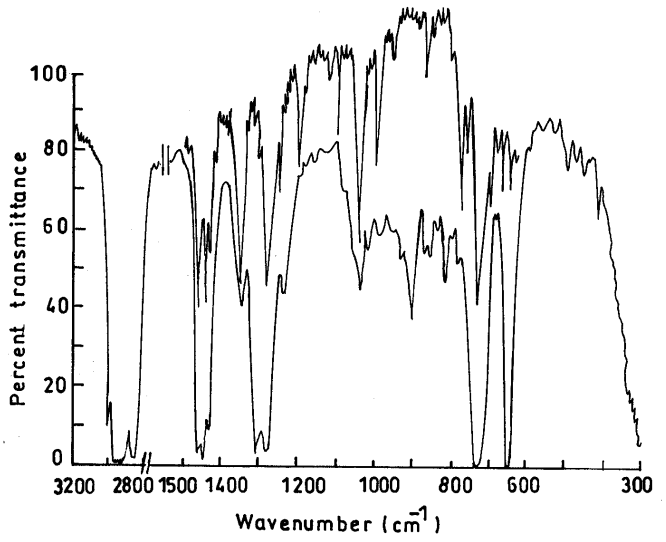

Figure 9.20 Infrared spectra of 1,6-dichlorohexane. Lower curve, liquid; upper curve, annealed solid at about 80K.

decades [77–79]. As n-alkanes and branched alkanes are generally liquids at ambient temperatures, they are expected to exist in many conformations; therefore, their vibrational (infrared and Raman) spectra in the liquid phase are a superposition of the spectra due to all the conformations. However, when the spectrum is recorded at subambient temperatures (at which these substances crystallize) it contains information for only one conformation—the most stable. The FT-IR spectrometer is a powerful tool for recording the infrared spectra of liquids at ambient temperatures and crystalline solids at subambient temperatures. This method has been used to make a complete assignment of observed bands to definite modes of vibrations in different conformations of some alkanes by normal coordinate calculations [80–82]. Jaggi and Jaiswal [83–87] have also carried out the vibrational analysis of some chloro-substituted alkanes. Figure 9.20 shows the infrared spectra recorded by the FT-IR spectrometer of 1,6-dichlorohexane in liquid as well as in crystalline phase.

9.4.6 Study of Bio-Molecules

In the analysis of bio-molecules such as proteins, the region of the spectrum that gives the greatest amount of information on structure and composition is usually the biological fingerprint region from 2000 cm^{-1} to 900 cm^{-1}. This region can be very well studied with FT-IR spectrometers. The fact that most proteins in their native state are in aqueous solution raises the problem of resolving the weaker protein absorption bands from the stronger

water absorption bands. One method of avoiding this problem is to use D_2O as the solvent instead of water. However, this defeats the original objective of observing the protein in native environment. Powell et al. [88] developed an important algorithm for the spectral subtraction of water from the FT-IR spectra of proteins in dilute solutions and observed monolayers, which is a very useful way to study biological molecules.

During recent years, FT-IR spectroscopy has been applied to a large number of problems in clinical chemistry. Due to improvements in spectrometric equipment and efficient data evaluation and software, more accurate and reliable analytical results are now obtained, compared to earlier studies. Heise et al. [89] gave an analytical multicomponent method for the blood substrates total protein, glucose, total cholesterol, triglycerides, and urea in human plasma by FT-IR spectroscopy. The obvious advantages are that, for this multicomponent method, no reagents apart from rinsing and cleaning agents are necessary. In addition, this method could be used for monitoring purposes.

Breast cancer is a worldwide and common disease whose fatal outcome can be prevented only by early diagnosis. Infrared techniques such as thermography and transmission imaging, which are based on infrared radiation emission and absorption between normal and diseased breast tissue, have already been used as clinical diagnostic tools for breast cancer. Wallon et al. [90] have applied near infrared spectroscopy to detect the presence of cancer cells in breast tissue in correlation with the pathological diagnosis. Zhang et al. [91] have recently applied cluster analysis and artificial natural networks (ANN) to the automated assessment of a disease state by Fourier transform infrared microscopic imaging measurements of normal and carcinomatous human breast cells.

Sowa and Mantsch [92] have utilized rapid scan and step-scan-based FT-IR photoacoustic techniques for depth profiling of an extracted but intact human tooth. As photoacoustic detection is not directly affected by light scattering or high optical sample density, the mineral phase of intact calcified tissues can be nondestructively characterized. In addition, photoacoustic depth profiling can potentially provide information on the interaction between the mineral phase and the underlying protein matrix during tissue mineralization.

9.4.7 Study of Polymers

Polymers are present in our every day life, having different morphologies such as films, powders, or fibers [93]. Koeing described numerous applications of FT-IR spectroscopy to study a variety of polymer systems. O'Neil and Fateley [94] reviewed the achievements of Koeing in the field of polymer science. Koeing has been a remarkable leader in the field of polymer systems. His innovative use of various modern spectroscopic techniques

including FT-IR has revolutionized the understanding of the characterization of polymer systems. The research has greatly influenced work in basic structural measurements of newly discovered polymers to quality control measurements of polymers. He had also carried out the vibrational analysis of polymers by recording the vibrational spectra of polymers. In the determination of structure of various polymers, FT-IR technique has been a very useful analytical method. But with the development of FT-IR microspectroscopy, detailed analysis of the spatial distribution of chemical species at the fiber-matrix interphase can be performed. Recently Arvanitopoulos and Koeing [95] applied this technique to study the interphase of glass fiber-epoxy composites.

Polyethylene terphthalate (PET) is one of the most widely utilized industrial polymer materials. Detailed knowledge about structures and physical properties of the polymer is indispensable for its application to industrial products such as base films of magnetic tapes, plastic bottles, synthetic fibers, and so on. Investigation of the surface structure of PET film has been conducted with an attenuated total reflection method [96] and by Sonoyama et al. [33] by dynamic step-scan two-dimensional Fourier transform infrared studies. Very recently Kandilioti et al. [97] made the conformational analysis of this polymer.

REFERENCES

[1] Ghatak, A.K., Goyal, I.C. & Chua, S.J. (1995) *Mathematical Physics* New Delhi: MacMillan Academic Press.

[2] Harper, C. (1993) *Introduction to Mathematical Physics* New Delhi: Prentice-Hall of India Private Ltd.

[3] Arfken, G. (1985) *Mathematical Methods for Physicists* Orlando: Academic Press, Inc.

[4] Lee, J.P. & Comisarow, M.B. (1987) *Appl. Spectrosc*. **41**, 93-98.

[5] Steward, E.G. (1983) *Fourier Optics: An Introduction* New York: John Wiley & Sons.

[6] Banwell, C.N. & McCash, E.M. (1999) *Fundamentals of Molecular Specroscopy* New Delhi: Tata McGraw-Hill Publishing Co. Ltd.

[7] Guelachvili, G. (1981) *Spectroscopic Techniques*; G. A. Vanasse; Volume **II** New York: Academic Press.

[8] Berry, A., www.FT-IR.htm

[9] www. ericweisstein.com

[10] Bacsik, Z., Mink, J. & Keresztury, G. (2004) *Appl. Spectrosc. Reviews* **39**, 295-363.

[11] Codding, E.G. & Horlick, G. (1973) *Appl. Spectrosc.* **27**, 85-92.

[12] Lipp, E.D. (1986) *Appl. Spectrosc*. **40**, 1009-1011.

[13] Kawata, S., Noda, T. & Minami, S. (1987) *Appl. Spectrosc*. **41**, 1176-1182.

[14] James, D.I., Maddams, W.F. & Tooke, P.B. (1987) *Appl. Spectrosc*. **41**, 1362-1370.

[15] Kauppinen, J.K., Moffatt, D.J., Mantsch, H.H. & Cameron, D.G. (1981) *Appl. Spectrosc*. **35**, 271-276.

[16] Aruldhas, G. (2004) *Molecular Structure and Spectroscopy* New Delhi, Prentice- Hall of India Private Ltd.

[17] Green, D.W. & Reedy, G.T. (1978) *Fourier Transform Infrared Spectroscopy Applications to Chemical Systems Vol. 1*, Ferraro, J.R. & Basile; L.J., p18–38 New York, Academic Press.
[18] Grasselli, J. (1987) *Appl. Spectrosc.* **41**, 933-935.
[19] Bell, R.J. (1972) *Introductory Fourier Transform Spectroscopy* New York, Academic Press.
[20] Cooley, J.W. & Tukey, J.W. (1965) *Math. Comput*. **19**, 291.
[21] Connes, J. & Connes, P. (1966) *J. Opt. Soc. Am*. **56**, 896-910.
[22] Connes, P., Connes, J. & Maillard, J.P. (1969) *Atlas des Spectres dans le Proche Infrarouge de Venus, Mars, Jupiter, et Saturne* Paris: Editions des Centre National de Recherche Scientifique.
[23] Jacquinot, P. (1969) *Appl. Optics* **8**, 497-499.
[24] Gibbie, H.A. (1969) *Appl. Optics* **8**, 501-504.
[25] Horlick, G. & Yuen, W.K. (1978) *Appl. Spectrosc*. **32**, 38-46.
[26] Koeing, J.L. (1975) *Appl. Spectrosc*. **29**, 293-308.
[27] Hirschfeld, T. (1976) *Appl. Spectrosc.* **30**, 68-69.
[28] www.photometrices.net
[29] Hoffmann, P. & Knözinger, E. (1987) *Appl. Spectrosc.* **41**, 1303-1306.
[30] Thackeray, P.P.C. (1972) *Laboratory Methods in Infrared Spectroscopy* Miller, R.G.J., Stace, B.C., p 8 London; Heyden and Son Ltd.
[31] Kember, D., Chenery, D.H., Sheppard, N. & Fell, J. (1979) *Spectrochimica Acta.* **35A** 455-459.
[32] Manning, C.J. & Griffiths, P.R. (1997) *Appl. Spectrosc*. **51**, 1092-1099.
[33] Sonoyama, M., Shoda, K., Katagiri, G. & Ishida, H. (1996) *Appl. Spectrosc*. **50**, 377-381.
[34] Fellgett, P. (1958) *J. Phys. Radium* **19***,* 187.
[35] Voigtman, E. & Winefordner, J.D. (1987) *Appl. Spectrosc*. **41**, 1182-1184.
[36] Jacquinot, P. (1954) *Proceedings of the 17th Congress du Gaurs CNRS* (Paris)
[37] Koeing, J.L. (1975) *Appl. Spectrosc*. **29**, 293-308.
[38] Hirschfeld, T. (1985) *Appl. Spectrosc*. **39**, 1086-1087.
[39] Hirschfeld, T. (1986) *Appl. Spectrosc*. **40**, 1239-1240.
[40] Tripp, C.P. & McFarlane, R.A. (1994) *Appl. Spectrosc*. **48**, 1138-1142.
[41] Parry, D.B. & Harris, J.M. (1988) *Appl. Spectrosc*. **42**, 997–1004.
[42] Johnson, S.A., Rinkus, R.M., Diebold, T.C. & Maroni, V.A. (1988) *Appl. Spectrosc*. **42**, 1369-1375.
[43] Sergides, C.A., Chughtai, A.R. & Smith, D.M. (1987) *Appl. Spectrosc*. **41**, 157-160.
[44] Rahmelow, K. & Hübner, W. (1996) *Appl. Spectrosc*. **50**, 795-804.
[45] Maddams, W.F. (1980) *Appl. Spectrosc*. **34**, 245–267.
[46] Bowley, H.J., Collin, S.M.H., Gerrard, D.L., James, D.I., Maddams, W.F., Tooke, P.B. & Wyatt, I.D. (1985) *Appl. Spectrosc*. **39**, 1004-1009.
[47] Notingher, I., Imhof, R.E., Xiao, P. & Pascut, F.C. (2003) *Appl. Spectrosc.* **57**, 1494-1501.
[48] Cran, M.J. & Bigger, S.W. (2003) *Appl. Spectrosc*. **57**, 928-932.
[49] Markham, J.R., Best, P.E. & Solomon, P.R. (1994) *Appl. Spectrosc*. **48**, 265-270.
[50] Iwaoka, T., Tabata, F. & Tsutsumi, S. (1994) *Appl. Spectrosc*. **48**, 818-826.
[51] Lutz, E.T.G., Luinge, H.J., Maas, J.H. van der & Agen, R. van (1994) *Appl. Spectrosc*. **48**, 1021-1025.
[52] Ouyang, H., Sherman, P.J., Paschalis, E.P., Boskey, A.L. & Mendelsihn, R. (2004) *Appl. Spectrosc*. **58**, 1-9.
[53] Thompson, S.E., Foster, N.S., Johnson, T.J., Valentine, N.B. & Amonette, J.E. (2003) *Appl. Spectrosc*. **57**, 893-899.

[54] Horn, B.A., Qiu, J., Owen, N.L. & Feist, W.C. (1994) *Appl. Spectrosc*. **48**, 662-668.
[55] Chirsty, A.A., Nodland, E., Burnham, A.K., Kvalheim, O.M. & Dahl, B. (1994) *Appl. Spectrosc*. **48**, 561-568.
[56] Heberle, J. & Zscherp, C. (1996) *Appl. Spectrosc*. **50**, 588-596.
[57] Lewis, E.N., Gorbach, A.M., Marcott, C. & Levin, I.W. (1996) *Appl. Spectrosc*. **50**, 263-269.
[58] Sowa, M.G. & Mantsch, H.H. (1994) *Appl. Spectrosc*. **48**, 316-319.
[59] Conde-Gallardo, A., Cruz-Orea, A. & Tomas, S.A. (2004) *Appl. Spectrosc*. **58**, 917–921.
[60] Irudayaraj, J. & Tewari, J. (2003) *Appl. Spectrosc*. **57**, 1599-1604.
[61] Van de Voort, F.R., Sedman, J., Yaylayan, V., Laurcnt, C.S. & Mucciardi, C. (2004) *Appl. Spectrosc*. **58**, 193-198.
[62] Stewart, D. (1996) *Appl. Spectrosc*. **50**, 357-381.
[63] Hanst, P.L., Spiller, L.L., Watts, D.M., Spence, J.W. & Miller, M.F. (1975) *J. Air Pollut. Contr. Assoc.* **25**, 1220.
[64] Hanst, P.L. (1978) *Fourier Transform Infrared Spectroscopy Applications to Chemical Systems Vol. 2,* Ferraro, J.R., Basile, L.J. (Eds.), p 88–89 New York, Academic Press.
[65] Hong, D.W. & Cho, S.Y. (2003) *Appl. Spectrosc*. **57**, 299-308.
[66] Kraft, M., Jakusch, M., Karlowatz, M., Katzir, A. & Mizaikoff, B. (2003) *Appl. Spectrosc*. **57**, 591-599.
[67] Mantz, A.W. (1976) *Appl. Spectrosc*. **30**, 459-461.
[68] Fink, U. & Larson, H.P. (1978) *Fourier Transform Infrared Spectroscopy Applications to Chemical Systems Vol. 2,* Ferraro, J. R. Basile; L.J., p 247–253, 259 New York, Academic Press.
[69] Ochiai, S., McClelland, J.F., Kobayashi, K. & Takaoka, K. (1994) *Appl. Spectrosc.* **48**, 1287-1289.
[70] Yamamoto, K. & Ishida, H. (1994) *Appl. Spectrosc*. **48**, 775-787.
[71] Ohta, K. & Iwamoto, R. (1985) *Appl. Spectrosc*. **39**, 418-425.
[72] Fredericks, P.M., Samson, P.J. & Stuart, A.D. (1987) *Appl. Spectrosc*. **39**, 327-329.
[73] Lowry, S., May, T., Bornstein, A., Weissman, Y., Harman, R. & Tugenthaft, I. (1994) *Appl. Spectrosc*. **48**, 852-856.
[74] Poirier, M.A., Lopes, T. & Singh, B.R. (1994) *Appl. Spectrosc*. **48**, 867-870.
[75] Steiner, H., Jakusch, M. & Kraft, M. et al. (2003) *Appl. Spectrosc*. **57**, 607-613.
[76] Katzir, A. & Mizaikoff, B. (2003) *Appl. Spectrosc*. **57**, 823-828.
[77] Schachtschneider, J.H. & Snyder, R.G. (1963) *Spectrochimica Acta*. **19**, 117-168.
[78] Snyder, R.G. & Schachtschneider, J.H. (1965) *Spectrochimica Acta*. **19**, 169-195.
[79] Schachtschneider, J.H. (1964) *Shell Development Co. Tech. Repts*. 231-264.
[80] Jaiswal, R.M.P. & Crowder, G.A. (1983) *Candian J. Spectrosc*. **28**, 160-164.
[81] Crowder, G.A. & Jaiswal, R.M.P. (1983) *J. Mol. Struct.* **102**, 145-164.
[82] Crowder, G.A. & Jaiswal, R.M.P. (1983) *J. Mol. Struct.* **99**, 93-100.
[83] Jaggi, N. & Jaiswal, R.M.P. (2002) *Ind. J.Pure & Appl. Phys.* **40**, 385-392.
[84] Jaggi, N. & Jaiswal, R.M.P. (2002) *Ind. J. Phys.* **76B**, 297-306.
[85] Jaggi, N. & Jaiswal, R.M.P. (2001) *Ind. J. Pure & Appl Phys.* **39**, 123-129.
[86] Jaggi, N. & Jaiswal, R.M.P. (2000) *Ind. J. Phys.* **74B**, 493-496.
[87] Jaggi, N. & Jaiswal, R.M.P. (2000) *Ind. J. Pure & Appl Phys.* **38**, 69-80.
[88] Powell, J.R., Wasacz, F.M. & Jakobsen, R.J. (1986) *Appl. Spectrosc.* **40**, 339-344.
[89] Heise, H.M., Marbach, R., Koschinsky, T.H. & Gries, F.A. (1994) *Appl. Spectrosc.* **48**, 85-95.
[90] Wallon, J.W., Yan, S.H., Tong, J., Meurens, M. & Haot, J. (1994) *Appl. Spectrosc.* **48**, 190-193.
[91] Zhang, L., Small, G.W., Haka, A.S., Kidder, L.H. & Lewis, E.N. (2003) *Appl. Spectrosc.* **57**, 14-22.

[92] Sowa, M.G. & Mantsch, H.H. (1994) *Appl. Spectrosc.* **48**, 316-319.
[93] Papini, M. (1994) *Appl. Spectrosc.* **48**, 472-476.
[94] O'Neil, S.E. & Fateley, W. (1988) *Appl. Spectrosc.* **42**, 1177-1180.
[95] Arvanitopoulos, C.D. & Koeing, J.L. (1996) *Appl. Spectrosc.* **50**, 1-10.
[96] Walls, D. (1991) *Appl. Spectrosc.* **45**, 1113.
[97] Kandilioti, G., Govaris, G.K. & Gregoriou,V.G. (2004) *Appl. Spectrosc.* **58**, 1082-1092.